2009

Planar Microscale Ionization Devices in Atmospheric Air with Diamond-Based Electrodes

D. B. Go
Purdue University - Main Campus

T. S. Fisher
Purdue University - Main Campus

S V. Garimella
Purdue University, sureshg@purdue.edu

V. Bahadur
Purdue University - Main Campus

Go, D. B.; Fisher, T. S.; Garimella, S V.; and Bahadur, V., "Planar Microscale Ionization Devices in Atmospheric Air with Diamond-Based Electrodes" (2009). *CTRC Research Publications*. Paper 128.
http://dx.doi.org/10.1088/0963-0252/18/3/035004

Planar microscale ionization devices in atmospheric air with diamond-based electrodes

D B Go[1], T S Fisher , S V Garimella, V Bahadur
School of Mechanical Engineering and Birck Nanotechnology Center, Purdue University, West Lafayette, Indiana 47907 USA

ABSTRACT

Planar microscale ionization devices that operate in atmospheric air have been developed out of highly graphitic polycrystalline diamond (HGPD). The devices have been fabricated on both silicon and quartz substrates with electrode gaps ranging from 5 to 20 μm. Experiments show that the HGPD devices operate in the pre-breakdown regime where a field emission mode enables appreciable ionization current without the occurrence of sparks or breakdown. The devices are compared to prior experiments with HGPD thin-films, and these new, on-chip devices operate at similar current magnitudes of 100 nA to 5 μA. For comparison, titanium planar ionization devices have also been fabricated and tested. However, these devices were unable to operate at any appreciable current without the formation of spark discharges. These results suggest that HGPD is a good candidate material for integrated, on-chip ionization devices for applications including miniature mass spectrometry, gas sensing, and microscale electrohydrodynamics.

[1] Corresponding author and currently Assistant Professor, Department of Aerospace and Mechanical Engineering, University of Notre Dame, Notre Dame, Indiana 46556, USA email: dgo@nd.edu

1. INTRODUCTION

Recent studies of the ionization of atmospheric air have focused on the breakdown phenomenon which occurs at microscale dimensions, where two electrodes exposed to air are spaced less than 20 μm apart. Much of this recent interest has been driven by the design of microelectromechanical systems (MEMS) where closely-spaced electrodes are operated at applied potentials ranging from the hundreds to thousands of volts (for instance – in electrostatic actuators). The breakdown of air in the interstitial gaps between electrodes is an unintended and often damaging consequence of these higher-voltage MEMS. However, microscale ionization devices at atmospheric pressure also have the potential to be applied to various on-chip technologies including miniature mass spectrometers ([1]-[3]), ionization gas sensors ([4]-[6]), and heat transfer enhancement devices ([7],[8]). One goal in developing microscale ionization devices for these applications is to operate them below the breakdown threshold while still generating appreciable ion current. This is because breakdown at atmospheric pressures is often accompanied by undesired sparking and arcing, electrode damage due to ion bombardment, and unsteady ion currents. The present work introduces a planar, on-chip microscale ionization device using highly graphitic polycrystalline diamond (HGPD) that generates appreciable ion current in atmospheric air without breakdown of the air.

Paschen conducted one of the earliest studies of electrical breakdown in gaseous environments when he derived his classic breakdown relationship between the applied voltage, the gaseous pressure, and the distance (or gap) between the electrodes [9]. Breakdown occurs when the formation of an electron avalanche leads to over-exponential carrier (ions and electrons) multiplication. At atmospheric pressure, this is often accompanied by space charge effects resulting in streamer formation and glow or spark discharges [10]. The breakdown criterion, commonly called Paschen's law, can be written as

$$V_b = \frac{Bpd}{\ln\left(\frac{Apd}{\ln\left(1+1/\gamma\right)}\right)} \qquad (1)$$

where V_b is the breakdown voltage, p is the pressure, d is the gap, γ is Townsend's second ionization coefficient, and A and B are constants based on the electrode materials and interstital gases in question.

One of the major consequences of Paschen's law is its prediction of breakdown as a function of gap size. In atmospheric air, as the gap reduces to approximately 5-10 μm, Paschen's curve reaches a minimum

value, and then the breakdown voltage begins to increase as the gap continues to decrease. The reason for the voltage minimum is that as the gap decreases, electron loss to the boundaries overwhelms electron generation either by ionization (called an α process) or by secondary emission from the electrodes due to bombardment (called γ processes), unless additional energy (*i.e.*, voltage) is added to the system. However, in the past decade, a number of experimental studies have suggested that Paschen's curve does not accurately describe the processes in microscale gaps, and the breakdown voltage does not reach a minimum but continues to decrease as the gap separation decreases.

Torres and Dhariwal [11] and Lee *et al*. [12] both used point-to-plane configurations in which one electrode is suspended above the other and separated by an air gap. They each studied different electrode materials (copper, brass, iron, aluminum and nickel [11], iron and silver [12]) and observed deviation from Paschen's curve below 5 μm. Slade and Taylor [13] evaluated the experimental results and concluded that, at microscale gaps, electron field emission injects electrons into the gas, thereby overcoming electron loss to the boundaries and allowing the breakdown voltage to decrease. Zhang *et al.* [14] confirmed this hypothesis using a particle-in-cell Monte Carlo (PIC-MC) computational technique that incorporated a field emission component to match the observed experimental trends. More recently, others have continued to study microscale ionization theoretically ([15]-[19]).

In addition to the classic point-to-plane configuration, discharges in microscale gaps have been studied for more practical electrodes integrated on the surface of a substrate in a planar configuration. Ono *et al*. [20] studied interdigitated silicon (Si) electrodes on a Si substrate. They considered two configurations: one where both electrodes were Si, and a second where one of the Si electrodes was uncoated and the other was coated with a thin chromium-gold (Cr-Au) metal layer less than 20 nm thick. The breakdown voltages of the Si-to-Si electrodes were consistent with Paschen's curve even with gaps as small as 2 μm, while the Si-to-metal electrodes deviated from Paschen's curve below 7 μm. Additionally, deposits left on the anode in the Si-to-Si configuration appeared to be consistent with the sputtering of material from the cathode by ion bombardment. Wallash and Levitt [21] also observed a deviation from Paschen's curve in air using planar chrome electrode structures on glass. In their work, they suggested a modified form of the breakdown curve that follows Paschen's law for electrode gaps greater than 10 μm, goes through a transition "plateau" from a Paschen's breakdown to field emission between 5-10 μm, and below 5 μm is linear and due

purely to field emission. Experimentally, they showed that the plateau occurs between 2-4 μm suggesting that field emission dominates the other processes for gaps below 2 μm, and they also observed damage to their electrodes after breakdown. Chen *et al.* [22] studied planar, inter-digitated p-type and n-type Si electrodes on silicon-on-insulator (SOI) substrates and aluminum (Al) electrodes on glass substrates. They also observed that the Si electrodes actually followed Paschen's curve with the doping only affecting the minimum breakdown voltage, whereas the Al electrode deviated from Paschen's curve as observed by others using metal electrodes. Both the Si and Al electrodes also showed damage accumulated during breakdown. Strong *et al.* [23] recently studied specifically designed shapes for planar, polysilicon electrodes on Si substrates. They investigated tip diameters ranging from 2-20 μm at gaps from 2-7 μm, and suggested that processing and surface roughness play significant roles in affecting the local electric field because of geometric effects. They also precisely characterized the nature of the discharge currents and concluded that their electrodes experienced traditional Townsend discharge avalanches rather than field emission.

As suggested above, field emission plays an important role in ionization in microscale gaps, and recently, researchers have studied various materials and small-scale features for both vacuum and atmospheric emission ([24]-[26]). Gröning *et al*. [27] studied diamond as a possible material because of its presumed negative electron affinity (NEA) and suggested that films with low resistivity, high defect density, and the presence of many grain boundaries have favorable emission properties. Additionally, the high thermal conductivity and mechanical strength of diamond make it a good electrode material for ionization processes where bombardment damage can be significant as shown in [20]-[22] and [24].

Prior work in the authors' group has considered various carbon-based materials, including highly graphitic polycrystalline diamond (HGPD) and carbon nanotubes (CNTs), for low-voltage ionization in air (Peterson *et al*. [28]). Using a point-to-plane configuration, it was demonstrated that HGPD (as grown on a tungsten substrate) operated at appreciable currents (1-100 μA) and low voltages (< 400 V) without breakdown occurring in the air gap. The study concluded that HGPD is an attractive material for low-voltage ionization of atmospheric air below the breakdown threshold. Figure 1 shows a comparison of the results from Peterson *et al*. [28] to Paschen's curve, as well as some representative experimental data on microscale ionization. The shaded area in the figure highlights the region of potential operation for HGPD-based devices.

The present work describes the development of a planar, highly graphitic polycrystalline diamond (HGPD) microscale ion generation device with electrode gaps ranging from 5 to 20 μm. Fabrication processes have been developed for HGPD devices on both Si and quartz wafers, demonstrating the potential of this material in different applications. The performance of the HGPD devices is compared to the performance of titanium (Ti) electrodes as a representative conventional material.

2. DEVICE OVERVIEW AND EXPERIMENTAL METHOD

2.1 Device Overview

The basic geometry of the planar, microscale ion generation devices considered in this work consists of two electrodes in an interdigitated arrangement (Figure 2). Each electrode has a large rectangular contact pad for application of a micromanipulator probe. Protruding from each contact pad is an electrode finger. The fingers from the electrode pair have an overlapping region that is the active ionization region. The device was designed with interdigitated electrodes so that probe contact on the contact pads did not influence the ionization. The electrode gap in the active region ranged from 5 to 20 μm, and the overlapping length of the active region was 1000 to 1500 μm. The electrode widths ranged from 10 to 100 μm, and the thickness of the electrode ranges from 0.5 to 1.5 μm depending on the material of the electrode and the deposition method.

Both the HGPD and Ti devices were fabricated on both Si and quartz substrates for comparison in order to demonstrate the suitability of the devices to different applications. A 1 μm layer of thermally grown silicon dioxide (SiO_2) on the surface of the Si substrate was used to electrically isolate the electrodes, while no special insulating layer was required for the quartz substrates. The Ti devices were fabricated by sputter-depositing a Ti thin-film, approximately 500 nm thick, and patterning it using standard photolithography techniques. The metal layer was wet-etched using hydrofluoric acid buffered in ammonia at a 1:6 ratio. Because Ti electrodes are fabricated by surface processes, the above method is applicable to both Si and quartz substrates. The fabrication of HGPD requires different processes for the Si and quartz substrates, and the details are discussed in Section 3.

2.2 Experimental Method

Electrical tests were conducted in dc mode by bringing two micromanipulator probes into contact with each contact pad of the ionization device. One of the probes was connected to a Keithley 6485 picoammeter and grounded, while the other probe was connected to a high-voltage power supply. (In this study, two different power supplies were used – a Spellman CZE1000 was used for voltages greater than 300 V while a Sorenson DHP was used for voltages less than 300 V because it offered finer voltage control) The voltage was incremented slowly over a period of approximately 10 to 30 minutes while the transient current response was recorded with Keithley software. The tests were conducted inside a transparent plastic enclosure in order to prevent cross-drafts from affecting the results, and on an optical table to mitigate the influence of vibrations. The results from Ti devices are presented in Section 4.1 and compared to theory. The results from HGPD devices were compared to point-to-plane measurements by Peterson *et al.* [28] for HGPD thin-films on tungsten (W) and to new point-to-plane measurements for HGPD thin-films on Si. In this work, 'thin film' refers to a substrate that has complete HGPD coverage in contrast to the present ionization devices which consist of electrodes patterned from a thin film.

3. DEVELOPMENT OF HGPD DEVICES

3.1 Overview of HGPD Growth

In this work, HGPD is grown using a Seki Technotron Corporation AX5200 Series microwave plasma chemical vapor deposition (MPCVD) system. The MPCVD consists of a vacuum chamber in which the plasma is ignited and maintained by a microwave frequency power source. Methane (CH_4) is used as the carbon-containing gas, and hydrogen (H_2) is used as the gas that couples to the plasma and promotes diamond growth by scavenging some of the non-diamond carbon deposits. The growth substrate is placed on a molybdenum (Mo) puck, which is in turn placed on a vertical translation stage that can be positioned at an optimal height for stable plasma generation. The stage is heated inductively to a set target temperature, and a dual-wavelength pyrometer is used to monitor the surface temperature of the wafer. The housing of the vacuum chamber is grounded, and the stage can be biased either positively or negatively. If the stage is not biased, it has a floating potential relative to the positive plasma and grounded chamber. Details on the

geometry and general operation of this MPCVD system were described previously by Maschmann *et al.* [31].

The basic growth procedure for HPGD thin films using bias-enhanced nucleation is documented in [28]. For the point-to-plane measurements, HGPD was grown on Si substrates with no SiO_2 insulating layer. General growth parameters are listed in Table 1 for HGPD on Si, and Figure 3 shows a representative scanning electron microscope (SEM) image of HGPD growth on Si. Many sharp grain boundaries and facets on the surface of the thin-film were observed, and these features favorably enhance the local electric field for field emission.

3.2 Patterned HGPD Electrodes on Si and Quartz Substrates

The challenge in developing HGPD devices is that the HGPD must be grown on either a dielectric layer (such as SiO_2 on Si) or on a dielectric substrate (such as quartz) so that the electrodes are electrically isolated. However, in practice, growth on SiO_2 or quartz proved to be difficult. In this work, growth and patterning approaches were developed for both SiO_2 on Si substrates and quartz substrates.

For SiO_2 on Si substrates, a layer of Ti was deposited on the SiO_2 because it more readily nucleates HGPD. Additionally, based on exploratory tests to ensure complete HGPD coverage on the Ti layer, the Ti and SiO_2 had to be patterned to expose pure Si between the electrodes *prior to growth* as outlined in the fabrication steps (a)-(c) of Figure 4. The Ti was sputter-deposited and patterned using photolithography and hydrofluoric acid buffered in ammonia at a 1:6 ratio using the same approach discussed above for the Ti electrode devices. A reactive ion etch (RIE), using tetrafluoromethane (CF_4) and octafluorocyclobutane (C_4F_8) in an oxygen plasma, was used to vertically etch the SiO_2 to expose the Si without etching the Ti layer.

Using the MPCVD parameters listed in Table 1, HGPD film was successfully grown on the $Ti/SiO_2/Si$ substrates. Figure 5 shows a SEM image (top view) of representative growth on a Si wafer that had three different regions that were exposed to the plasma: exposed Si, exposed SiO_2 on the Si, and exposed Ti on top of the SiO_2 layer. HGPD grew as continuous films on both the exposed Si and the exposed Ti regions. However, a continuous HGPD film did not form in areas where SiO_2 was exposed; rather sparse microclusters of HGPD were formed. This microcluster growth phenomenon on SiO_2 is similar to that

observed by others who have developed diamond-based field emission devices [32]. Figure 5 confirms the fabrication and growth methodology proposed in Figure 4 to synthesize HGPD on an insulating layer. In the development of final devices there was no exposed SiO_2. Raman spectroscopy was used to evaluate the HGPD growth on the Ti electrodes as shown in Figure 6. The peak at 1335 cm^{-1} represents the sp^3 bonding character indicative of diamond. A second peak at 1580 cm^{-1} represents sp^2 bonding character, and the broadened shoulder between the sp^3 and sp^2 peaks is indicative of significant graphite-like content in addition to diamond ([33],[34]).

After HGPD growth, aluminum (Al) was used as a metal mask for the HGPD on the Ti electrodes. The Al was deposited by thermal evaporation and patterned using photolithography and a phosphoric acid/acetic acid/nitric acid/deionized water solution (80:5:5:10 ratio) etchant. The exposed HGPD was then etched using an oxygen (O_2) and sulfur hexafluoride (SF_6) plasma, and finally the Al was stripped to reveal the final devices.

HGPD growth on quartz never resulted in a film coverage, but resulted in either no growth or the same sparse microclusters previously observed on SiO_2 layers. One of the primary reasons postulated for poor HGPD growth on quartz is that a sufficient carbide layer is not formed during the nucleation step. Therefore, the implemented process used a thin film of a material that favors the formation of carbide as a nucleation layer to initiate growth. Titanium, silicon carbide (SiC) and Si were all tested as potential nucleation layers with varying degrees of success – only the Si nucleation layer consistently produced HGPD films. In addition to using a nucleation layer, a molybdenum (Mo) clip was used to form a conductive path from the Mo puck in the MPCVD to the nucleation layer. The Mo clip allowed the nucleation layer to be biased directly during growth, thus bypassing any electrical insulation effects of the quartz substrate. Figure 7 shows a representative SEM image of the HGPD grown on quartz substrates using a 400 nm, sputter-deposited Si nucleation layer and the growth parameters in Table 1. The fabrication of HGPD devices from the thin-film on quartz is very similar to the latter steps (d)-(f) for HGPD on Si shown in Figure 4. Figure 8 shows SEM images of a fabricated HGPD ionization device on a quartz substrate.

4. RESULTS AND DISCUSSION

4.1 Ti Ionization Devices

On both the Si and quartz substrates, the Ti devices were unable to maintain an appreciable current (defined as > 100 nA) without transitioning into breakdown with visible discharges and sparking. Figure 9 shows a representative device with a 15 μm gap in the active region before and during the experiment with the breakdown discharges clearly visible. The curved features at the end of the electrode arms represent one of the design elements that was used to minimize the effect of field concentration around tips and edges. Notably, the discharges were formed in the active region of the devices, indicating that the contact pads and probe tips did not influence operation. Additionally, while this particular image shows a relatively uniform discharge, localized sparking was also observed.

The Ti devices performed similarly on both the Si and quartz substrates. Figure 10 compares the breakdown voltage (defined as the voltage where the monitored current quickly transitioned from the sub-nA range to greater than 50 μA and upwards of hundreds of μA) for four different electrode gaps (5, 10, 15, and 20 μm) to the predicted breakdown voltage from Paschen's law. The experimental data follow the trends predicted by Paschen's curve, and significant deviation from Paschen's law was not observed. This result can likely be attributed to both poor emission properties of the Ti and the electrode geometry such that field-emitted electrons were not injected into the air, though devices with electrode gaps smaller than 5 μm would be needed to confirm this hypothesis. Additionally, the Ti electrodes experienced significant damage due to the electron and ion bombardment as was found in past studies on microscale breakdown ([20]-[22]).

4.2. HGPD Ionization Devices

Figure 11 shows a representative current versus applied potential plot for an HGPD ionization device on a Si substrate with a 10 μm gap. As opposed to the Ti devices that only had sub-nA currents prior to breakdown, the HGPD device demonstrated appreciable current that increased steadily with voltage and reached a maximum near 1 μA. Additionally, no breakdown of the air was observed for the potential range tested, and therefore the current never transitioned to very high values. Therefore, it appears that the HGPD device is operating below the breakdown threshold (as suggested in **Figure 1**) in an ionization regime akin to

the non-self-sustaining discharge regime [35]. However, the exponential shape of the curve also suggests that field emission is occurring.

According to traditional discharge theory, in the non-self-sustaining discharge regime, ionization occurs at first via random events and then predominantly through electron impact ionization. The current will initially increase with voltage until it reaches a saturation state where the current remains constant as the voltage increases. As the voltage approaches the breakdown voltage (Paschen's curve), an electron avalanche forms and the current rapidly increases by orders of magnitude – a phenomenon that was observed for the Ti devices. However, for the HGPD devices, the current steadily increases with increasing voltage, and this can be directly attributed to the role of field emission. The non-self-sustaining, steady current i can be written as [35]

$$i = i_o e^{\alpha d} \Big/ \left[1 - \gamma\left(e^{\alpha d} - 1\right)\right], \tag{2}$$

where i_o is the emission current from the cathode, α is Townsend's first ionization coefficient, γ is Townsend's secondary ionization coefficient, and d is the electrode gap. The Fowler-Nordheim equation describes the field emission electron current as a function of voltage [36], and by substituting in the Fowler-Nordheim for the emission current i_o, the total current can now be expressed as

$$i = \left(\frac{e^{\alpha d}}{\left[1 - \gamma\left(e^{\alpha d} - 1\right)\right]}\right) \cdot \left(\frac{C_1 \Phi^2}{C_2}\right) \exp\left[-\frac{C_3}{C_4 \Phi}\right], \tag{3}$$

where $C_{1\text{-}4}$ are constants associated with the electrode material (the work function) and geometry as well as other constants related to field emission (see [37] for more details on the Fowler-Nordheim equation), and Φ is the applied potential. Eq. 3 describes the ionization current due to field emission from the cathode and can be written in a more general, linear form relating the current and applied potential

$$\ln\left(\frac{i}{\Phi^2}\right) = f\left(\frac{1}{\Phi}\right). \tag{4}$$

If a negative slope is observed when plotting this relationship, then it is apparent that field emission is the primary cathode electron source for pre-breakdown ionization (note that an analogous relationship is often used to confirm vacuum field emission [38]). Figure 12 shows a plot of Eq. (4) for the same 10 μm device above, and the strong linear relationship (the superimposed linear fit) at voltages greater than 20 V ($1/\Phi$ = 0.05 V^{-1}) adds confidence that field emission is indeed prominent. However, the data are not perfectly linear

especially at lower applied potentials ($1/\Phi > 0.05\ V^{-1}$), suggesting that field emission likely does initiate below 20 V, and this very low-voltage current is due to random events common in a non-self-sustaining discharge.

Figure 13 shows the variation of current with applied potential for three different HGPD ionization devices on Si for gaps of 10, 15, and 20 μm, as well as data from Peterson *et al.* [28]. As is evident, the performance of the present HGPD electrodes is comparable to potential-current performance of the HGPD thin film tested by Peterson *et al.* [28] with maximum currents of approximately 1-5 μA for the applied potential range tested. Two separate ramps for the same 20 μm device are also shown in Figure 13. The first curve is the first test and the second curve (labeled 'subsequent') was obtained after a number of tests on the same device. The degradation of the device over time is evident from the differences between the current versus applied potential characteristics in both magnitude and trend. It is also apparent that there is no discernable impact of the electrode gap on the measured current. These two observations are likely due to the fact that surface properties that affect electron emission from the HGPD, and thus emission current, are not well controlled in the HGPD growth processes. Local surface properties including active emission sites on the HGPD, surface contamination, and geometric electric field enhancement cannot be identified directly, but affect emission and also can vary over time.

In contrast to the Ti devices, visible arcing and sparks were not observed in the potential range tested for any of the HGPD devices. Figure 14 shows microscope images of a Ti device after 10 minutes of operation where sparking occurred and an HGPD device after forty hours of continuous operation. Figure 14a shows the severe erosion of Ti electrodes due to the ion and electron bombardment during these highly energetic sparking events - consistent with others' observations of erosion for iron and silver [12], Si, platinum [20], chrome [21], and aluminum [22]. In contrast, the HGPD electrodes (Figure 14b) suffered only minor damage, particularly in the gap between the electrodes and on the edges where SiO_2 was exposed. **Figure 15** shows an SEM image of the edge of an HGPD electrode after testing. There is visible damage near the edge of the HGPD, likely due to ion bombardment, but no apparent damage on the HGPD itself – which was also confirmed by higher magnification images of the HGPD (not shown). The robustness of the HGPD electrodes is likely the result of their inherent material properties (hardness, chemical stability, and high thermal conductivity) and their operating regime. Because they prevent breakdown, HGPD electrodes also

operate at lower voltages, and therefore, at lower bombardment energies and currents. While some of the Ti devices experienced damage ultimately leading to failure, no HGPD device suffered catastrophic failure from bombardment.

A number of similar experiments were conducted using HGPD devices on quartz substrates. The following results are for a 5 μm gap device over a number of tests, and are representative of typical results for larger gap spacings. Figure 16 shows the nominal (averaged over four tests) current as a function of applied potential for the device. Unlike the HGPD on Si devices, this device reached a peak current of only 45 nA at 300 V, and the response did not show the exponential shape expected for field emission, suggesting that a Townsend discharge was the dominant phenomenon. After subsequent experiments, the device degraded and eventually settled at a current of ~2 nA for applied potentials as high as 300 V.

Hydrogen plasma treatments have been known to help improve the emission characteristics of diamond and HGPD films ([27], [28], [39]). While the exact effect of the treatment is not well established, it is postulated that the plasma cleans the surface of the film of impurities, and the surface becomes hydrogen-terminated, thus reducing the electron affinity. The HGPD-on-quartz wafer was therefore placed into the MPCVD chamber and treated with a 500 W, 100 sccm H_2 plasma at 15 torr and a Mo puck temperature of 500 ºC (the quartz surface temperature was approximately 620 ºC) for 30 minutes. Figure 17 shows the results of 12 hr endurance tests at 300 V after each H_2 plasma treatment along with a point-to-plane endurance test using a continuous HGPD thin-film on a pure Si substrate. The point-to-plane measurement was conducted with a 10 μm air gap and a constant applied potential of 600 V. After the first H_2 plasma treatment, the 5 μm planar device operated at an emission current of approximately 200 nA – a two orders of magnitude improvement over the untreated device. The second plasma treatment improved the operating current of the device by a factor of two. Note that the 5 μm device exhibited greater currents than its HGPD thin-film counterpart. Additionally, the current response showed unsteady characteristics for the duration of the test, consistent with the work of Peterson *et al.* [28].

These results demonstrate that H_2 plasma treatments can be used to improve the performance of HGPD ionization devices, though it is not expected that repeated plasma treatments would continue to improve the device performance because the performance of the HGPD would reach some limiting threshold. The endurance tests also suggest that HGPD can operate in a regime below the breakdown

threshold with appreciable current for extended time periods, though further work is required to improve the stability of the current. Finally, consistent with the HGPD on Si devices, there was no damage due to electron or ion bombardment observable on these HGPD electrodes.

5. CONCLUSIONS

Highly graphitic polycrystalline diamond (HGPD) planar, microscale ionization devices have been fabricated on both Si and quartz substrates and are compared to titanium (Ti) devices. The Ti devices did not generate any appreciable ion current with increasing voltage until the breakdown of air and sparking and microdischarges were observed. In contrast to Ti, sparking and microdischarge breakdown was not observed using HGPD ionization devices. The HGPD devices operated in a pre-breakdown regime where a field-emission mode which allowed for appreciable ion current without the occurrence of breakdown. While further study is required to fully control the emission and performance capabilities of the HGPD, particularly to ensure long-term stability, this work highlights the importance of materials selection in the design of microscale ionization devices and suggests HGPD as a viable, controllable ion source for gas sensing, miniature mass spectrometry, and other applications.

ACKNOWLEDGEMENTS

The authors wish to acknowledge Dr. Wei Zhang, Mr. Ratnakar Karru, and Mr. Raul A. Maturana who contributed to the development and testing of HGPD thin-films and devices. The authors would like to thank Mr. Vishal Mahulkar for assistance in capturing the images in **Figure 9**. The authors also acknowledge Intel Corporation for financial support.

REFERENCES

[1] Kornienko O, Reilly P T A, Whitten W B, and Ramsey J M 2000 *Anal. Chem.* **72** 559-62

[2] Hauschild J-P, Wapelhorst E, and Müller J 2007 *Int. J. Mass Spec.* **264** 53-60

[3] Debatin M, Kröner M, Mikosch J, Trippel S, Morrison N, Reetz-Lamour M, Woias P, Wester R, and Weidemüller M 2008 *Phys. Rev. A* **77** 033422

[4] Longwitz R G, van Lintel H, and Renaud P 2003 *J. Vac. Sci. Technol. B* **21** 1570-73

[5] Lim H H, Park D, Maeng J Y, Hwang J, and Kim Y J, 2006 *19th IEEE International Conference on Micro Electro Mechanical Systems* (Istanbul, Turkey) p 62-5

[6] Chua B, Wexler A S, Tien N C, Niemeier D A, and Holmen B A 2008 *J. Microelectromech. Syst.* **17** 115-123

[7] Go D B, Garimella S V, Fisher T S, and Mongia R K 2007 *J. Appl. Phys.* **102** 053302

[8] Schlitz D, Garimella S and Fisher T 2004 *ASME Heat Transfer/Fluids Engineering Summer Conference* (Charlotte, NC) 56470

[9] Paschen F 1889 *Ann. Phys.* **273** 69

[10] Nassar E 1971 *Fundamentals of Gaseous Ionization and Plasma Electronics* (New York: Wiley-Interscience) p 225-226

[11] Torres J-M and Dhariwal R S 1999 *Nanotechnology* **10** 102-7

[12] Lee R-T, Chung H-H, and Chiou Y-C 2001 *IEE Proc. – Science, Measurement and Technolgoy* **148** pp 8-14

[13] Slade P G and Taylor E D 2002 *IEEE Trans. Compon. Packag. Technol.* **25** 390-396

[14] Zhang W, Fisher T S, and Garimella S V 2004 *J. Appl. Phys.* **96** 6066-72

[15] Radmilović-Radjenović M, Lee J K, Iza F, and Park G Y 2005 *J. Phys. D: Appl. Phys* **38** 950-4

[16] Radmilović-Radjenović M and Radjenović B 2007 *Plasma Sources Sci. Technol.* **16** 337-40

[17] Radmilović-Radjenović M and Radjenović B 2007 *IEEE Trans. Plasma Sci.* **35** 1223-8

[18] Radmilović-Radjenović M and Radjenović B 2008 *Plasma Sources Sci. Technol.* **17** 024005

[19] Radmilović-Radjenović M and Radjenović B 2008 *Europhysics Lett.* **83** 25001

[20] Ono T, Sim D Y, and Esashi M 2000 *J. Micromech. Microeng.* **10** 445-51

[21] Wallash A and Levit L 2003 *Proc. SPIE* vol. 4980 p 87-96

[22] Chen C-H, Yeh J A, and Wang, P-J 2006 *J. Micromech. Microeng.* **16** p 1366-73

[23] Strong F W, Skinner J L, and Tien N C 2008 *J. Micromech. Microeng.* **18** 075025

[24] Wong T K S and Ingram S G 1993 *J. Phys. D: Appl. Phys* **26** 976-85

[25] Zhu W, Bower C, Kochanski P, and Jin S 2001 *Solid-State Electron.* **45** 921-28

[26] Kang W P, Fisher T S, and Davidson J L 2001 *New Diamond and Frontier Carbon Tech.* **11** 129-46

[27] Gröning O, Nilsson L-O, Gröning P, and Schlapbach L 2001 *Solid-State Electron.* **45** 929-44

[28] Peterson M S, Zhang W, Fisher T S, and Garimella S V 2005 *Plasma Sources Sci. Technol.* **14** 654-60

[29] Maxfield F and Benedict R 1941 *Theory of Gaseous Conduction and Electronics* (New York: McGraw-Hill)

[30] Siebert P, Petzold G, Hellenbart Á, and Müller J 1998 *Appl. Phys. A: Mater. Sci. Process* **67** 155-60

[31] Maschmann M R, Amama P B, Goyal A, Iqbal Z, Gat R, and Fisher T S 2006 *Carbon* **44** 10-18

[32] Kang W P, Davidson J L, Wisitsora-at A, Howell M, Jamaludin A, Wong Y M, Soh K L, and Kerns D V 2003 *J. Vac. Sci. Technol. B* **21** 593-6

[33] Yunjun L, Jintian H, Ning Y, and Binglin Z 1997 *10th International Vacuum Microelectronics Conference Technical Digest* (Kyongju, Korea) p 137-40

[34] Wisitsora-at A, Kang W P, Davidson J L, Kerns DV, and Fisher T S, 2003 *J. Vac. Sci. Technol. B* **21** 614-7

[35] Raizer Y P 1991 *Gas Discharge Physics* (New York: Springer-Verlag) p 130-3

[36] Fowler R and Nordheim L 1928 *Proc. R. Soc. London, Ser. A* **119** 626-39

[37] Go D B, Fisher T S, and Garimella S V 2009 *J. Phys. D: Appl. Phys.* **42** 055203

[38] Walker D G, Harris C T, Fisher T S, and Davidson J L 2005 *Diamond Related Matls.* **14** 113-20

[39] Robinson V S, Show Y, Swain G M, Reifenberger R G, and Fisher T S 2006 *Diamond Related Matls.* **15** 1601-8

LIST OF TABLES

Table 1 Typical MPCVD growth parameters for HGPD thin films on Si substrates, HGPD devices on Si substrates, and HGPD devices on quartz substrates for the experiments conducted in this work. For all processes the pressure was 15 torr.

	Thin-film on pure Si substrates		**Devices on Si or quartz substrates**	
Growth Parameter	**Nucleation**	**Growth**	**Nucleation**	**Growth**
H_2:CH_4 (sccm)	200:10	200:6	100:5	100:1
Mo puck T (°C)	690	690	700	700
substrate surface T (°C)	not available	not available	800-900	800-900
plasma power (W)	400	1000	300	300
dc bias (V)	-250	-125	-250	-125
time (hrs)	2:00	8:00-12:00	0:20-1:00	1:00-1:30

LIST OF FIGURES

Figure 16 Current as a function of applied potential for an HGPD ion generation device on a quartz substrate with a gap of 5 μm.

Figure 17 Current as a function of time for an HGPD ion generation device on a quartz substrate with a gap of 5 μm under a constant applied potential of 300 V for 12 hours, and a point-to-plane experiment with HGPD thin-films on Si using a 10 μm gap.

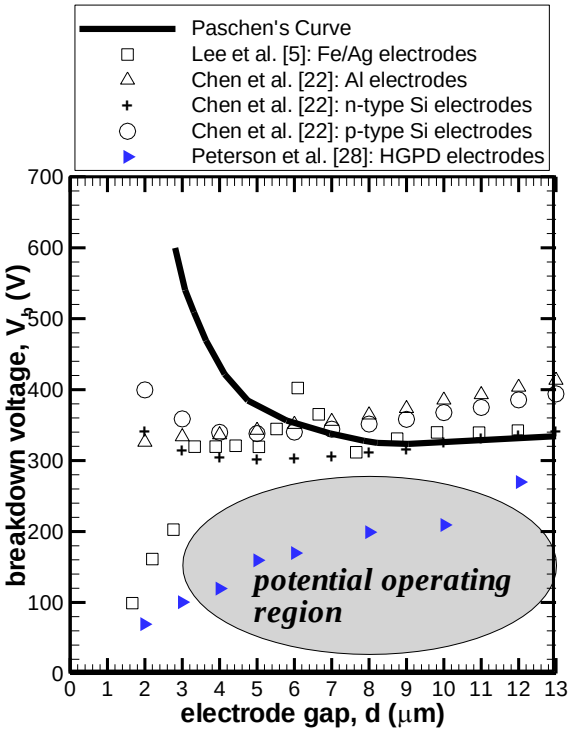

Figure 1 Comparison between traditional Paschen's curve for an iron cathode surface [29], electrical breakdown voltage measurements for microscale gaps reported by Lee *et al.* [5], breakdown voltage measurements for planar electrodes in an interdigitated, comb arrangement from Chen *et al.* [22] and the turn-on voltage curve measured by Peterson *et al.* [28]. The figure highlights the proposed operating regime for planar, microscale ionization devices below the breakdown threshold.

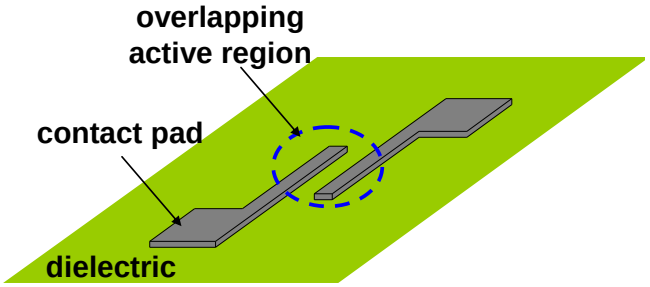

Figure 2 Schematic diagram of a planar, microscale ion generation device.

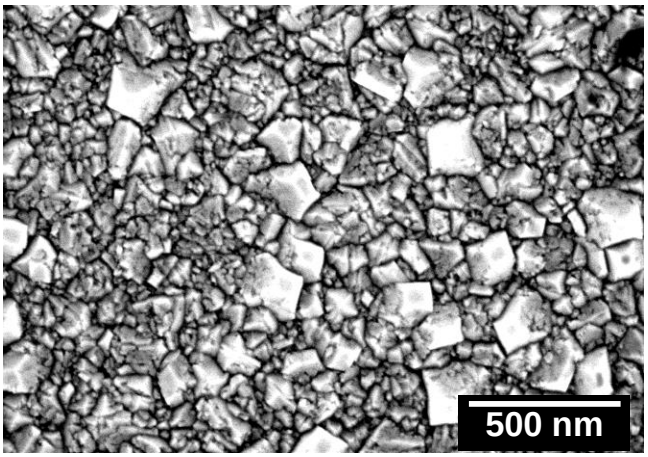

Figure 3 Scanning electron microscope (SEM) image of a representative diamond film on a Si substrate.

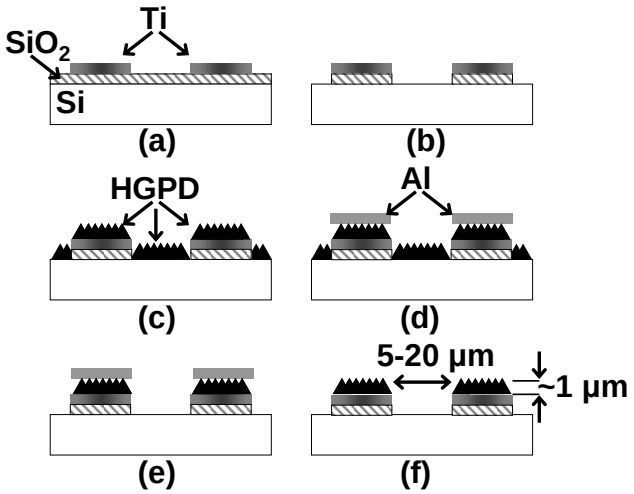

Figure 4 Schematic cross-sections of fabrication process for planar, microscale ionic wind engine with HGPD electrodes. (a) Si wafer with ~500 nm of deposited Ti on 1 μm of thermally grown, native SiO_2. (b) Wafer after RIE etch of SiO_2. (c) Wafer after MPCVD growth of HGPD. (d) Wafer after deposition and patterning of ~1 μm of Al. (e) Wafer after RIE etch of HGPD. (f) Final wafer after deposited Al layer is etched. The images are not to scale.

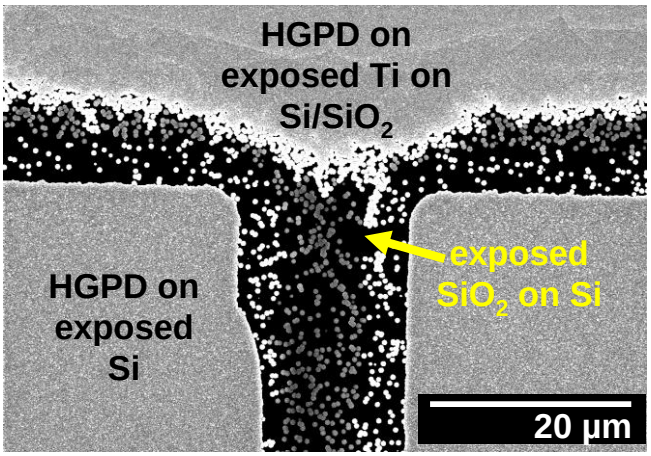

Figure 5 SEM image (top view) of representative HGPD growth on a Si wafer with three different regions exposed to the plasma: exposed Si substrate, SiO_2 on the Si substrate, and Ti on the SiO_2 layer on the Si substrate.

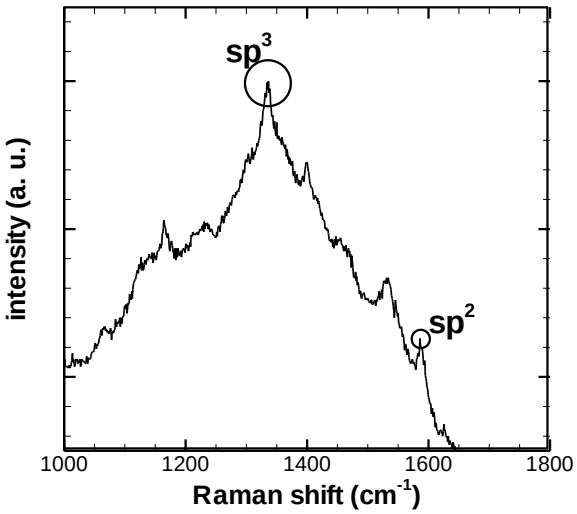

Figure 6 Raman spectrum for HGPD grown on a Ti/ SiO_2 /Si substrate. The Raman spectrum was obtained with a 783 nm LP Diode laser.

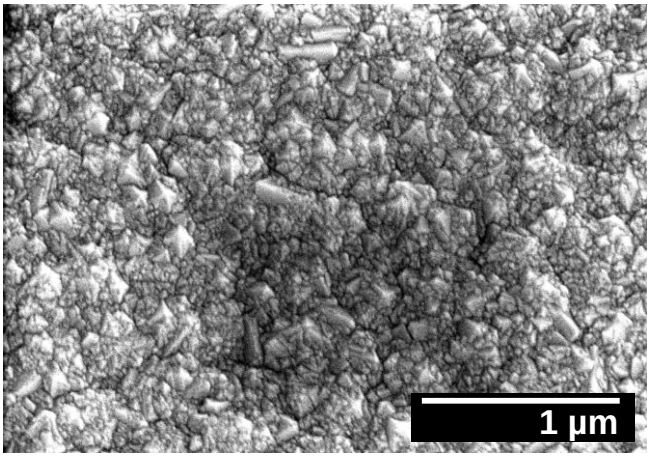

Figure 7 SEM image of a representative diamond film on a quartz substrate using a 400 nm Si nucleation layer and Mo clip.

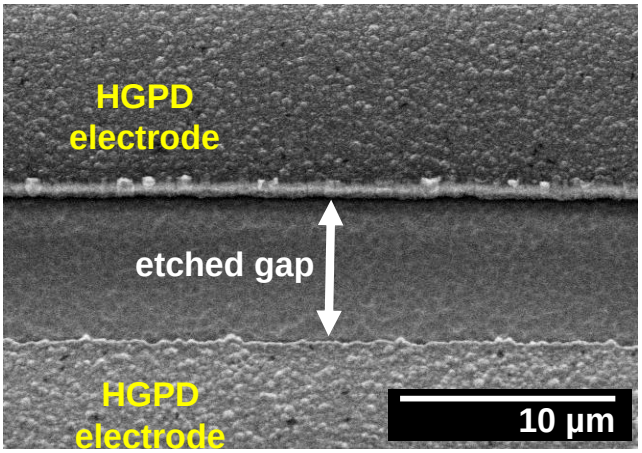

(a)

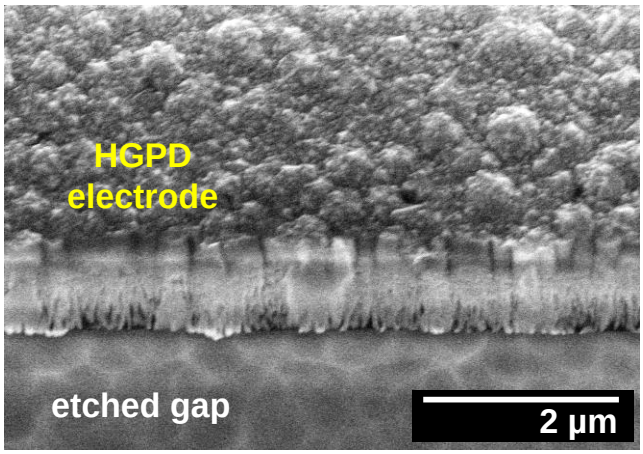

(b)

Figure 8 SEM images at two different magnifications of a fabricated HGPD ion generation device on a quartz substrate: (a) active region showing electrode gap with HGPD etched away, and (b) high-magnification view of electrode/gap interface.

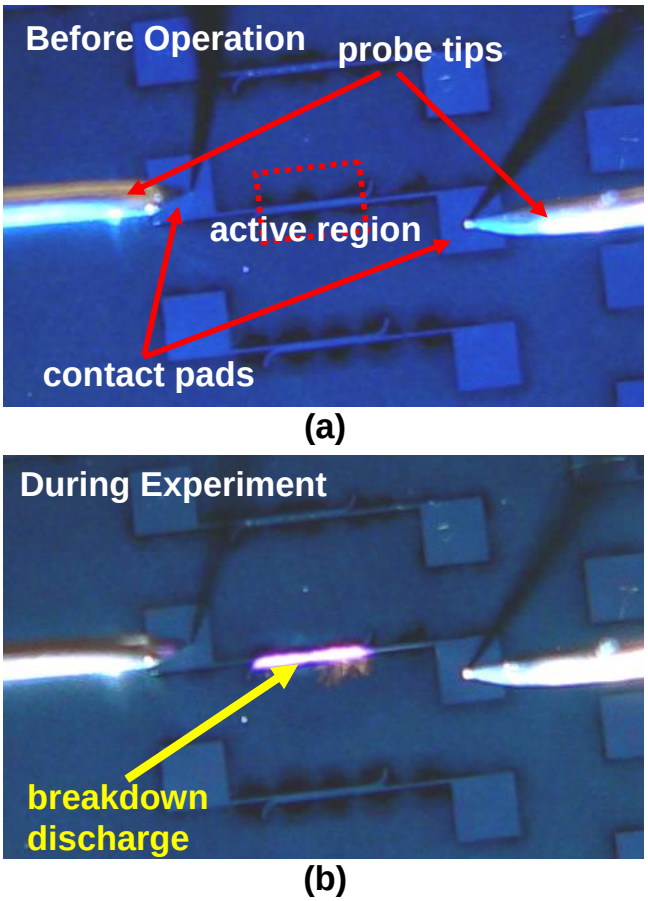

Figure 9 Image of Ti ion generation device on a Si substrate (a) before operation, and (b) during operation when breakdown occurs. The device gap is 15 μm.

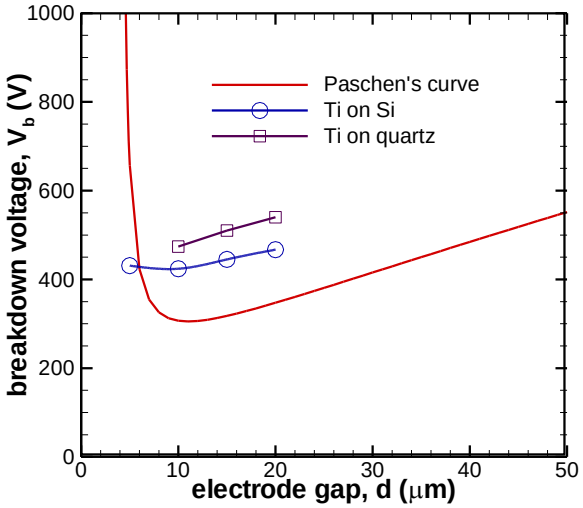

Figure 10 Experimental breakdown curve for Ti ion generation devices on Si and quartz substrates and qualitative comparison to Paschen's law.

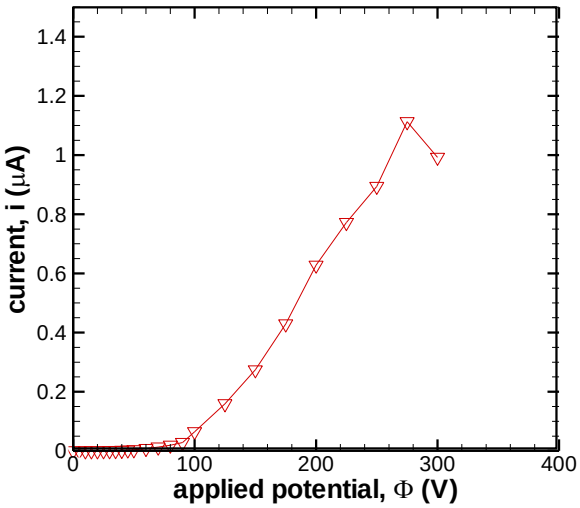

Figure 11 Current as a function of applied potential for an HGPD ion generation device on a Si substrate with a gap of 10 μm.

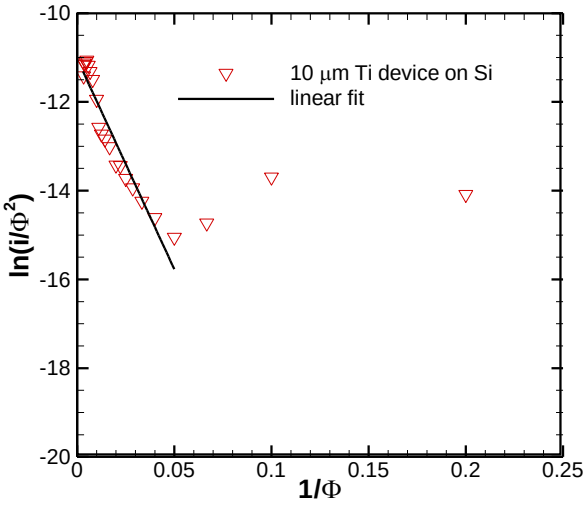

Figure 12 Fowler-Nordheim plot for an HGPD ion generation device on a Si substrate with a gap of 10 μm, and a linear curve fit superimposed on the data.

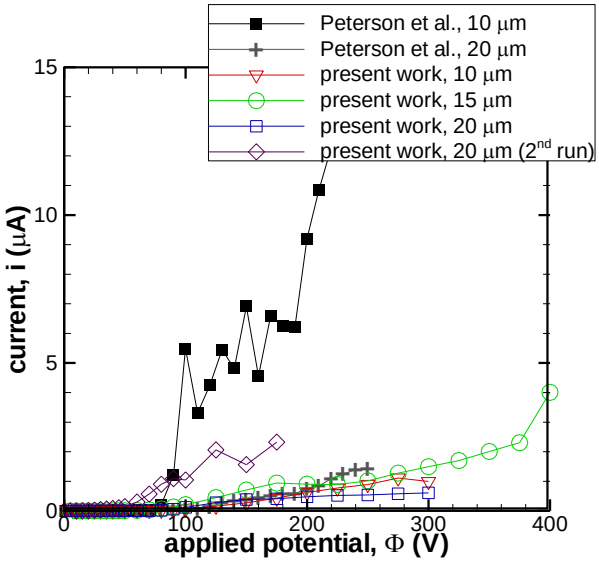

Figure 13 Current as a function of applied potential for three HGPD ion generation devices on a Si substrate and two data sets from [28].

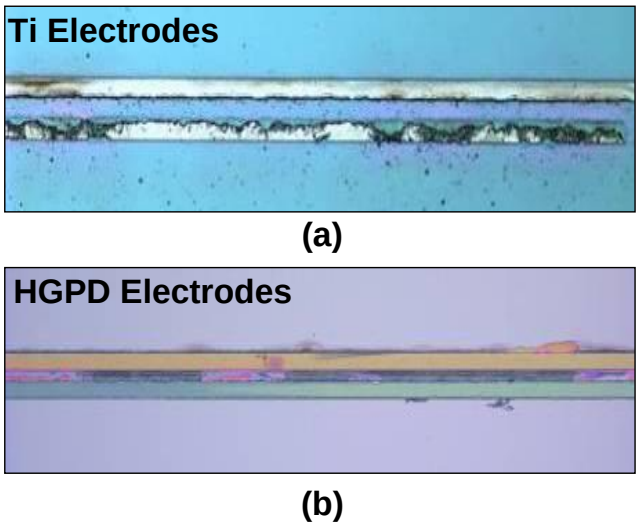

Figure 14 Microscope images of (a) Ti ion generation device on a Si substrate with a gap of 15 μm after 10 minutes of testing, and (b) HGPD ion generation device on a Si substrate with a gap of 10 μm after 40 hours of testing.

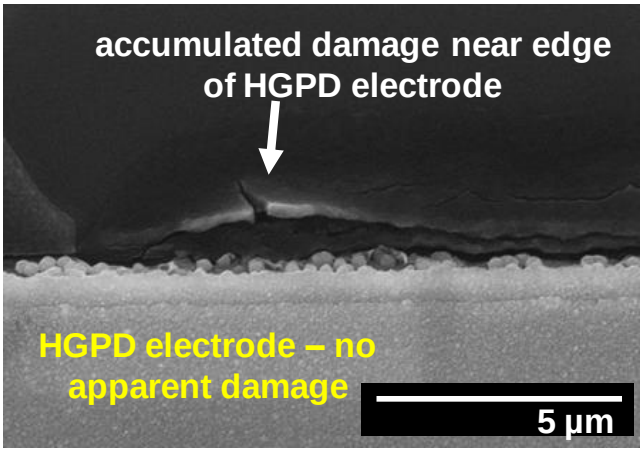

Figure 15 SEM image of HGPD ion generation device on a Si substrate after testing. There is visible damage near the edge of the HGPD electrode but no apparent damage on the HGPD itself.

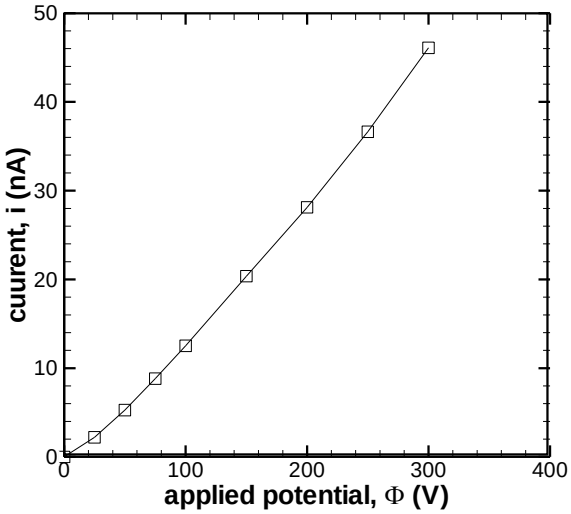

Figure 16 Current as a function of applied potential for an HGPD ion generation device on a quartz substrate with a gap of 5 μm.

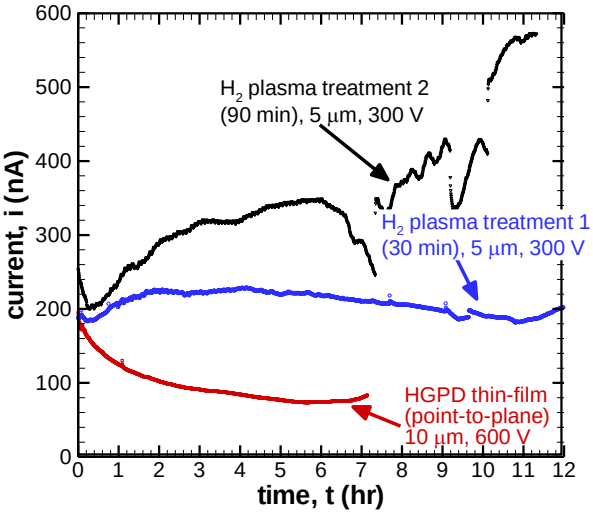

Figure 17 Current as a function of time for an HGPD ion generation device on a quartz substrate with a gap of 5 μm under a constant applied potential of 300 V for 12 hours, and a point-to-plane experiment with HGPD thin-films on Si using a 10 μm gap.